European Radiology (2019) 29:2293–2301
https://doi.org/10.1007/s00330-018-5911-3

MAGNETIC RESONANCE

Evaluation of renal dysfunction using texture analysis based on DWI, BOLD, and susceptibility-weighted imaging

Jiule Ding[1] · Zhaoyu Xing[2] · Zhenxing Jiang[1] · Hua Zhou[3] · Jia Di[3] · Jie Chen[1] · Jianguo Qiu[1] · Shengnan Yu[1] · Liqiu Zou[4] · Wei Xing[1]

Received: 7 June 2018 / Revised: 24 October 2018 / Accepted: 23 November 2018 / Published online: 17 December 2018

Abstract

Objective To explore the value of texture analysis based on diffusion-weighted imaging (DWI), blood oxygen level–dependent MRI (BOLD), and susceptibility-weighted imaging (SWI) in evaluating renal dysfunction.

Methods Seventy-two patients (mean age 53.72 ± 13.46 years) underwent MRI consisting of DWI, BOLD, and SWI. According to their estimated glomerular filtration rate (eGFR), the patients were classified into either severe renal function impairment (sRI, eGFR < 30 mL/min/1.73 m^2), non-severe renal function impairment (non-sRI, eGFR ≥ 30 mL/min/1.73 m^2, and < 80 mL/min/1.73 m^2), or control (CG, eGFR ≥ 80 mL/min/1.73 m^2) groups. Thirteen texture features were extracted and then were analyzed to select the most valuable for discerning the three groups with each imaging method. A ROC curve was performed to compare the capacities of the features to differentiate non-sRI from sRI or CG.

Results Six features proved to be the most valuable for assessing renal dysfunction: $0.25Quantile_{DWI}$, $0.5Quantile_{DWI}$, $Homogeneity_{DWI}$, $Entropy_{BOLD}$, $Skewness_{SWI}$, and $Correlation_{SWI}$. Three features derived from DWI ($0.25Quantile_{DWI}$, $0.5Quantile_{DWI}$, and $Homogeneity_{DWI}$) were smaller in sRI than in non-sRI; $Entropy_{BOLD}$ and $Correlation_{SWI}$ were smaller in non-sRI than in CG ($p < 0.05$). $0.25Quantile_{DWI}$, $0.5Quantile_{DWI}$, and $Homogeneity_{DWI}$ showed similar capacities for differentiating sRI from non-sRI. Similarly, $Entropy_{BOLD}$ and $Correlation_{SWI}$ showed equal capacities for differentiating non-sRI from CG.

Conclusion Texture analysis based on DWI, BOLD, and SWI can assist in assessing renal dysfunction, and texture features based on BOLD and SWI may be suitable for assessing renal dysfunction during early stages.

Key Points

- *Texture analysis based on MRI techniques allowed for assessing renal dysfunction.*
- *Texture features based on BOLD and SWI, but not DWI, may be suitable for assessing renal function impairment during early stages.*
- *SWI exhibited a similar capacity to BOLD for assessing renal dysfunction.*

Keywords Diffusion magnetic resonance imaging · Chronic kidney disease · Chronic renal insufficiency · Image processing, computer-assisted

Jiule Ding and Zhaoyu Xing contributed equally to this work.

Electronic supplementary material The online version of this article (https://doi.org/10.1007/s00330-018-5911-3) contains supplementary material, which is available to authorized users.

✉ Wei Xing
suzhxingwei@126.com; 840830590@qq.com

[1] Department of Radiology, Third Affiliated Hospital of Soochow University, Changzhou 213003, Jiangsu, China

[2] Department of Urology, Third Affiliated Hospital of Soochow University, Changzhou 213003, Jiangsu, China

[3] Department of Nephrology, Third Affiliated Hospital of Soochow University, Changzhou 213003, Jiangsu, China

[4] Department of Radiology, Shenzhen nanshan People's Hospital, Shenzhen University Health Science Center, Shenzhen 518000, Guangdong, China

Abbreviations

ADC	Apparent diffusion coefficient
AKI	Acute kidney injury
AUC	Area under the receiver operating characteristic curve
BOLD	Blood oxygen level–dependent MRI
CCC	Concordance correlation coefficient
CG	Control group
CI	Confidence interval
CKD	Chronic kidney disease
DWI	Diffusion-weighted imaging
eGFR	Estimated glomerular filtration rate
GLCM	Gray-level co-occurrence matrix
IQR	Interquartile range
MAD	Median absolute deviation
MRI	Magnetic resonance imaging
non-sRI	Non-severe renal function impairment
ROC	Receiver operating characteristic curve
sRI	Severe renal function impairment
SWI	Susceptibility-weighted imaging
T2WI	T2-weighted imaging

Introduction

Chronic kidney disease (CKD) still remains a major public health problem [1]. Evaluation of renal function in patients with hypertension and diabetes is very important, as they are common risk factors [1, 2]. It is believed that reduced perfusion, hypoxia, and renal fibrosis take part in the progression of renal impairment during the course of the disease [3, 4].

MRI imaging methods have been widely applied to assess different kidney diseases over the past decade including diffusion-weighted imaging (DWI), blood oxygen level–dependent MRI (BOLD), and susceptibility-weighted imaging (SWI) [5, 6]. These functional MRI imaging methods have shown great promise in assessing the renal function and renal fibrosis non-invasively. There is a relationship between renal function and water diffusion; thus, DWI may be suitable for evaluating renal function [7]. BOLD uses the endogenous magnetic properties of deoxyhemoglobin as a source of image contrast and could assess hypoxia that exists in the course of renal impairment. SWI is sensitive to venous oxygenation level as demonstrated in the cerebral veins during respiratory challenges like apnea or hyperventilation [8]. SWI successfully assessed pathological changes after renal ischemia-reperfusion injury and fibrosis during unilateral ureteral obstruction [6, 9].

MRI was commonly analyzed by using a sampling of several ROIs in the renal cortex and medulla. However, it is a tedious process and it does not quantify MRI signal heterogeneity of the human multi-lobar kidney. Texture analysis refers to the application of mathematical methods to evaluate the gray-level patterns and pixel interrelationship within an image [10, 11]. Texture analysis can quantify the level of organization of heterogeneity in images [11], like cortex-medulla contrast within the kidney. Several studies have suggested that texture features might be a new imaging biomarker in oncological imaging and staging of hepatic fibrosis [12, 13]. However, the assessment of renal dysfunction using texture analysis based on functional MRI is yet to be explored.

The primary objective of this study was to explore the value of texture analysis based on DWI, BOLD, and SWI in evaluating renal dysfunction.

Material and methods

Subjects

This retrospective study was approved by the local institutional review board (No. 2016-010), and written informed consent was obtained from all participants. From May 2013 to October 2017, 72 arterial hypertension or diabetes patients (52 males and 20 females, age ranging from 19 to 77 years, mean age 53.72 ± 13.46 years) with or without CKD were included. Arterial hypertension was defined as either (a) a mean office blood pressure of greater than 140/90 mmHg measured on more than one occasion or (b) an office blood pressure of less than 140/90 mmHg while taking one or more antihypertensive drugs. Diabetes was defined as either (a) a non-fasting blood glucose of 11.1 mmol/L or greater or (b) a fasting blood glucose of 7.0 mmol/L or greater [14]. CKD was defined as an estimated glomerular filtration rate (eGFR) of less than 60 mL/min per 1.73 m^2 or the presence of albuminuria (urine albumin-to-creatinine ratio > 100 mg/dL) for more than 3 months, irrespective of its cause. The exclusion criteria were as follows: (a) presence of kidney lesions (maximal diameter > 10 mm for any renal lesion or number of renal lesions > 5 in the right kidney), (b) breath-hold time < 13 s, (c) under 18 years old, and (d) acute renal function impairment [15].

The eGFR was calculated using Eq. 1: eGFR (mL/min/1.73 m^2) = $170 \times Scr^{(-0.999)} \times age^{(-0.176)} \times BUN^{(-0.170)} \times albumin^{(-0.318)} \times 0.762$ (if female), where age is in years, serum creatinine (Scr) is in mg/dL, blood urea nitrogen (BUN) is in mg/dL, and albumin is in g/dL. The eGFR was defined as 120 mL/min/1.73 m^2 if it was greater than 120 mL/min/1.73 m^2 as calculated using Eq. 1.

The subjects were classified into three groups: (1) a severe renal function impairment (sRI), where eGFR was < 30 mL/min/1.73 m^2; (2) a non-severe renal function impairment (non-sRI), where eGFR was ≥ 30 mL/min/1.73 m^2 but < 80 mL/min/1.73 m^2; and (3) a control group (CG), where eGFR was ≥ 80 mL/min/1.73 m^2.

MRI acquisition

All MRI images were acquired using 3.0 T (Magnetom Verio; Siemens Healthineers). The MRI sequences and the protocol are listed in Table 1. Coronal T2-weighted images were obtained for the anatomic identification. Then DWI, BOLD (T2*-weighted imaging with multiple echo times), and SWI were performed. The MRI examination was performed within 1 week. All subjects fasted for at least 3 h before undergoing MRI imaging.

An apparent diffusion coefficient (ADC) map was generated automatically using the DWI images at seven b-factors after the image coregistration embedded in the DWI protocol. ADC values were calculated in a pixel-by-pixel scheme by fitting the signal intensities on DWI images versus b-factor to a mono-exponential decay.

For BOLD imaging, T2* values were estimated as the slope of the decay rate of the MRI signal by fitting the signal intensity versus echo time to a single exponential function in a pixel-by-pixel scheme. A set of T2* maps was created, with each map corresponding to a specific slice.

For SWI imaging, a pair of magnitude and phase images, also known as high-pass filter–corrected phase images, was created. Then, a normalized phase mask was calculated from each corrected phase image and multiplied by the magnitude image four times to produce the final SWI image.

MRI image analysis

To avoid possible image artifacts resulting from air in the digestive tract, the imaging data of the right kidney was analyzed. The MRI images (one ADC map, one T2* map, and one SWI image per subject) at the central section through the renal hilum of the right kidney were selected for further analysis. The ROIs were initially delineated around the outline of the renal parenchyma by two radiologists who had more than 10 years of experience in abdominal MRI interpretation and were blinded to the clinical details (Fig. 1). The data measured by reader 1 (reader 1: J.C.) was considered for the main statistical analysis. To assess the inter-rater agreement of the texture features, 20 of the 72 subjects were sampled randomly, and their imaging data was analyzed by another radiologist (reader 2: J.G.Q.).

Texture analysis was conducted on the open-source software platform of Imaging Biomarker EXplorer (IBEX) [16]. Texture features from the gray-level histogram and the gray-level co-occurrence matrix (GLCM) were extracted from a single ROI for each subject. GLCM generated the texture features by comparing neighboring pixels for similarity and dissimilarity. The comparison was defined as a matrix $P\delta(i, j)$ to indicate the relative frequency, with gray levels of two pixels (i and j) at a distance ($\delta = 7$) and in a direction (0°). The seven texture features generated using the histogram method were Interquartile range (IQR_X), $Kurtosis_X$, Median absolute deviation (MAD_X), $0.25Quantile_X$, $0.5Quantile_X$, $0.75Quantile_X$, and $Skewness_X$; and, the six features generated using the GLCM method were $Contrast_X$, $Correlation_X$, $Energy_X$, $Entropy_X$, $Homogeneity_X$, and $Variance_X$, where $_X$ is one of the MRI imaging methods used (e.g., DWI, BOLD, or SWI). These 13 texture features may assist the radiologists in making diagnostic decisions [17–19].

Statistical analysis

Quantitative values were expressed as means ± standard deviation. To select the most valuable features for each imaging

Table 1 MRI protocol for renal dysfunction imaging

Sequence	T2WI	DWI	BOLD	SWI
Imaging plane	Coronal	Transverse	Coronal	Transverse
Breath technique	Breath-hold	Free-breath	Breath-hold	Breath-hold
TR/TE (ms)	2400/96	5300/96	112/3.00–43.56, in 6.76 ms steps	162/10
Field of view (mm^2)	380 × 380	380 × 285	360 × 270	380 × 285
Matrix	256 × 179	192 × 153	256 × 180	384 × 250
Number of slices	19	12	6	12
Slice thickness/gap (mm)	6.5/2.0	5.0/1.0	5.0/1.0	5.0/1.0
Flip angle (°)	160	–	60	15
Echo train length	179	EPI factor 115	–	–
Bandwidth (Hz/Px)	781	1184	490	620
b-factor (s/mm^2)	–	0, 20, 40, 80, 200, 400, 800	–	–
Scan time (s)	15	207	48	23

BOLD blood oxygen level–dependent MRI, *DWI* diffusion-weighted imaging, *T2WI* T2-weighted imaging, *TE* echo time, *TR* repeated time, *SWI* susceptibility-weighted imaging

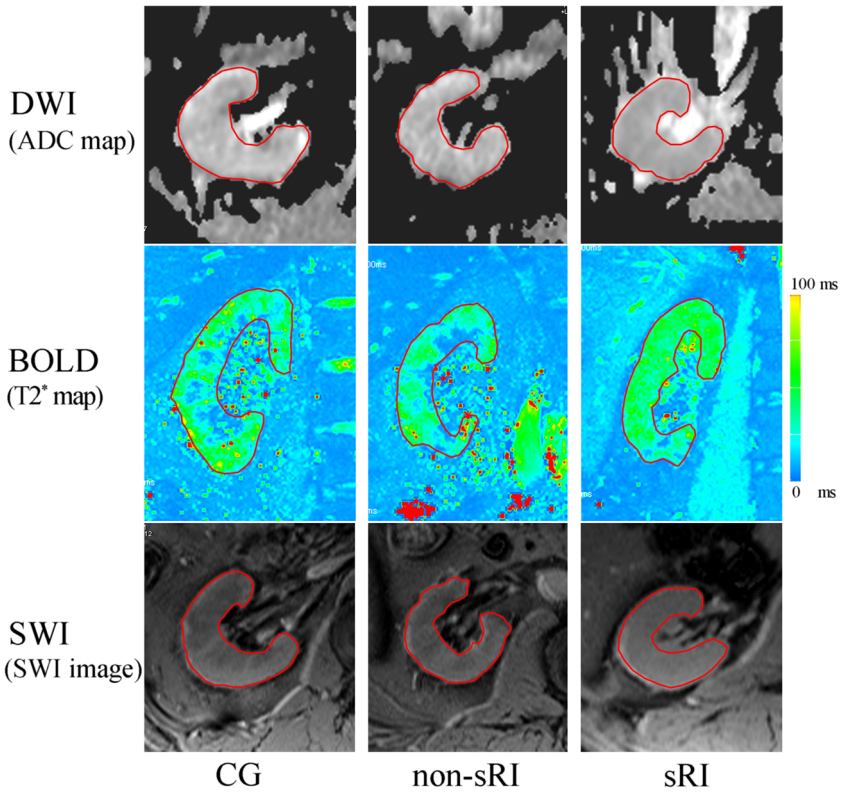

Fig. 1 Respective MRI images of the right kidney with or without renal dysfunction. The cortex-medulla contrast disappears with increased stage of renal dysfunction from control group (CG), non-severe renal function impairment (non-sRI), to severe renal function impairment (sRI). The regions of interest were curved over the renal parenchyma of the right kidney (red curve). In this study, the images analyzed were the apparent diffusion coefficient (ADC) maps for diffusion-weighted imaging (DWI), the T2* maps for blood oxygen level–dependent MRI (BOLD), and the susceptibility-weighted imaging (SWI) images for the SWI imaging method

method, the correlation of eGFR with the texture features was assessed using the Pearson coefficient. A random forest plot was performed to rank the importance of texture features that are used to classify the three groups using each MRI imaging method. The most valuable features had to meet the following criteria: (a) correlation coefficients with eGFR of >0.3 or <-0.3 (with $p<0.05$), which was considered as being of potential value in assessing renal dysfunction and (b) one of the top five important features listed in the mean decrease accuracy and also in the mean decrease Gini index for each imaging method, where the Gini index describes the overall explanatory power of the variables.

Inter-rater agreement was assessed for continuous variables using a concordance correlation coefficient (CCC) with a 95% confidence interval (95%CI). A CCC coefficient >0.7 indicates good inter-rater agreement.

One-way analysis of variance (ANOVA) was also performed to compare the age, eGFR, and texture features among sRI, non-sRI, and CG, and a Student-Newman-Keuls test was performed for all pairwise comparisons. The gender ratio among the three groups was compared using a chi-square test. The receiver operating characteristic curve (ROC) was used to compare the capacity of the selected texture features to differentiate non-sRI from sRI or CG. Pearson correlation, ANOVA, chi-square test, and ROC were performed using Prism 5 for Windows (Version 5.01, serial number: GPW5-384305-RAG-5235). The random forest plot and CCC were built or performed using R version 3.4.0 (Foundation for Statistical Computing, Tsinghua University). The statistical significance levels were reported to be two-sided for all analyses, with statistical significance set at 0.05.

Results

Comparison of patient characteristics

There were 31 subjects in sRI (male/female = 22/9 cases, 52.87 ± 13.64 years old, eGFR $= 16.47 \pm 6.03$ mL/min/1.73 m^2), 24 in non-sRI (18/6 cases, 52.67 ± 14.29 years old, 51.9 ± 16.99 mL/min/1.73 m^2), and 17 in CG (12/5 cases, 56.76 ± 12.19 years old, 101.0 ± 15.26 mL/min/1.73 m^2). The gender ratio and age showed no statistical difference among the three groups (chi-square = 0.139, $p=0.933$; $F=0.563$, $p=0.572$, respectively). The eGFR among the three groups was significantly different ($F=188.656$, $p<0.001$).

Selection of texture features

Of the 13 texture features for each imaging method, ten features exhibited significant correlations with eGFR for DWI (Table 2); one feature, $\text{Entropy}_{\text{BOLD}}$, for BOLD and two features, $\text{Skewness}_{\text{SWI}}$ and $\text{Correlation}_{\text{SWI}}$, for SWI (all $r>0.3$ or <-0.3). A random forest plot was performed to rank the importance of the features for each imaging method (Fig. 2). Potential valuable features were $0.25\text{Quantile}_{\text{DWI}}$,

Table 2 Correlation of eGFR with texture features based on DWI, BOLD, and SWI ($n = 72$)

Imaging method	DWI		BOLD		SWI	
	Pearson r	p	Pearson r	p	Pearson r	p
Contrast	− 0.307	0.009	0.009	0.942	− 0.216	0.069
Correlation	− 0.206	0.085	0.065	0.587	0.368	0.002
Energy	0.351	0.003	− 0.290	0.014	− 0.155	0.194
Entropy	− 0.391	< 0.001	0.391	< 0.001	0.254	0.031
Homogeneity	0.404	< 0.001	− 0.157	0.188	0.243	0.039
Variance	0.343	0.003	0.004	0.973	0.115	0.336
IQR	− 0.352	0.003	0.252	0.033	0.174	0.144
Kurtosis	0.366	0.002	0.102	0.395	− 0.154	0.196
MAD	− 0.330	0.005	0.261	0.027	0.160	0.180
0.25Quantile	0.447	< 0.001	0.002	0.986	− 0.081	0.498
0.5Quantile	0.381	0.001	0.117	0.329	− 0.065	0.587
0.75Quantile	0.292	0.013	0.160	0.179	− 0.025	0.833
Skewness	− 0.292	0.013	0.053	0.660	0.389	< 0.001

BOLD blood oxygen level–dependent MRI, *DWI* diffusion-weighted imaging, *eGFR* estimated glomerular filtration rate, *IQR* interquartile range, *MAD* median absolute deviation, *n* sample size, *SWI* susceptibility-weighted imaging

$0.5Quantile_{DWI}$, $Homogeneity_{DWI}$, and $Correlation_{DWI}$ for DWI; $Entropy_{BOLD}$, $0.5Quantile_{BOLD}$, and $Energy_{BOLD}$ for BOLD; and $Skewness_{SWI}$, $Entropy_{SWI}$, $Correlation_{SWI}$, and $Homogeneity_{SWI}$ for SWI. Thus, there were six most valuable features in total for the three imaging methods: $0.25Quantile_{DWI}$, $0.5Quantile_{DWI}$, $Homogeneity_{DWI}$, $Entropy_{BOLD}$, $Skewness_{SWI}$, and $Correlation_{SWI}$. The inter-rater agreement was good for these texture features (all CCC > 0.80, Table S1).

Comparison of texture features among sRI, non-sRI, and CG

The selected six texture features among sRI, non-sRI, and CG revealed significant differences between sRI and CG. And three features derived from DWI ($0.25Quantile_{DWI}$, $0.5Quantile_{DWI}$, and $Homogeneity_{DWI}$) were larger in non-sRI than in sRI. $Entropy_{BOLD}$ and $Correlation_{SWI}$ were larger in CG than in non-sRI (Table 3).

Capacity of texture features to differentiate non-sRI from sRI or CG

To compare the capacity of the selected six texture features to differentiate non-sRI from sRI or CG, ROC was performed (Table 4). The three features derived from DWI ($0.25Quantile_{DWI}$, $0.5Quantile_{DWI}$, and $Homogeneity_{DWI}$) all showed an ability to differentiate sRI from non-sRI (area under the receiver operating characteristic curve (AUC) = 0.827, 0.821, and 0.840, respectively) and showed no significant difference between their AUCs (Fig. 3a). $Entropy_{BOLD}$ and $Correlation_{SWI}$ showed the ability to differentiate non-sRI and CG and also showed no significant difference between their AUCs (Fig. 3b).

Discussion

Our data showed that several texture features derived from DWI, BOLD, and SWI were correlated with eGFR and enabled to differentiate sRI from CG. Furthermore, BOLD and SWI allowed discrimination of non-sRI from CG. DWI discriminated sRI from non-sRI.

Changes in DWI associated with renal dysfunction have been confirmed in several studies: ADC decreased in subjects with renal dysfunction, including CKD and acute kidney injury (AKI), compared with a control group [20–22]. However, the reasons for the decreased ADC values are complex. For CKD patients, ADC was significantly lower in most stages of CKD than in the normal group [20]. A negative correlation between ADC and serum creatinine (sCr) level has been found [20]. Although no interpretation was provided to explain the decreased ADC value in the CKD patients in Xu et al's study, renal fibrosis is probably one of the main causes [23]. In addition, DWI is also sensitive to blood flow changes [24, 25]. A significantly lower renal blood flow in both the renal cortex and medulla was observed in the CKD group compared to the control group [26]. Furthermore, the perfusion of both the renal cortex and whole kidney was correlated with eGFR ($r > 0.66$) [26, 27]. Therefore, another main cause of the decreased ADC in CKD patients is the reduction of renal perfusion. In contrast to clinical studies composed of CKD patients, the histological

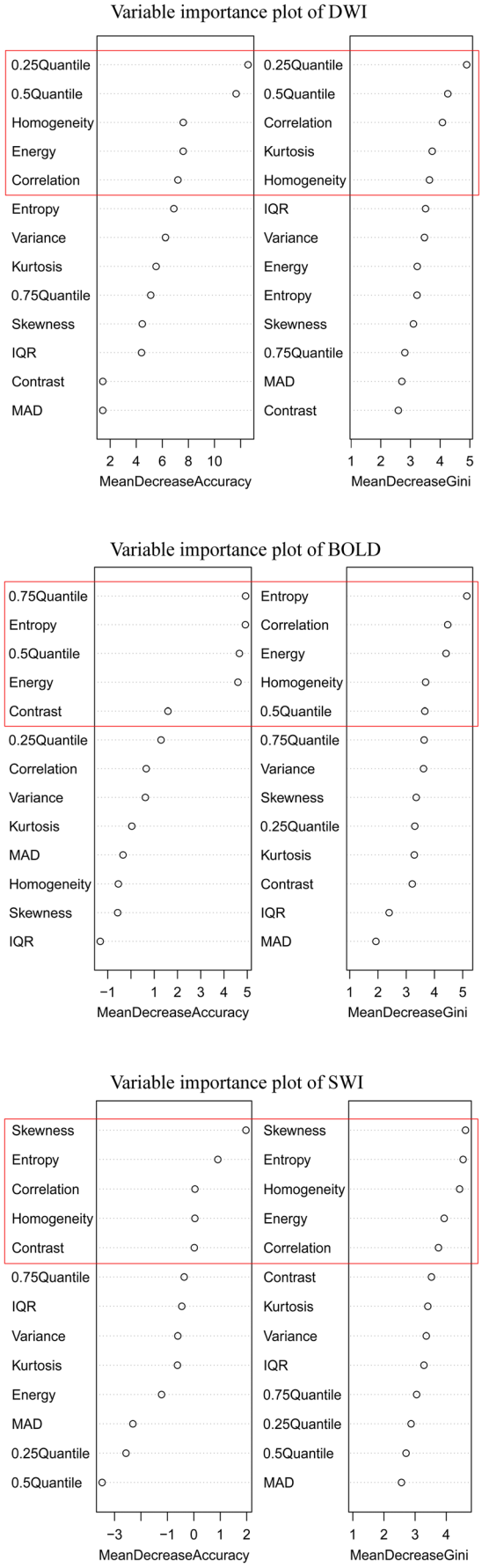

Fig. 2 Variable importance plot of texture features for discerning the control, non-severe renal function impairment, and severe renal function impairment groups. The variable important texture features are listed for each imaging method. The features for each imaging method are presented as the top five features in the mean decrease accuracy and also in the mean decrease Gini index (red box), where the Gini index describes the overall explanatory power of the variables

assessment was conducted easily in animal models of renal impairment. In Hueper's study, the medullary ADC was significantly reduced at all time points (days 0, 7, 14, and 28 post-AKI), whereas the degree of interstitial renal fibrosis increased until days 14 and 28 post-AKI [22]. In total, the decreased ADC over the progression of renal dysfunction may be attributed to the combination of reduced perfusion and interstitial fibrosis.

The role of BOLD in evaluating renal dysfunction has also been confirmed in several studies. A relative hypoxia is present in the renal medulla under normal conditions because the most energy-consuming tubular cells contain a great number of mitochondria with intense activity. This activity deteriorates over the course of renal injury, which was reflected indirectly by using BOLD [28]. As BOLD imaging provides a marker of blood oxygenation arising from the compound effect of perfusion, blood volume, and oxygen consumption [29, 30], there may not be a straightforward relationship between T2* (or R2*) measurement and oxygenation level [30, 31]. In the current study, a texture analysis of BOLD images showed a linear correlation with eGFR. To the best of our knowledge, the T2* value displayed a good correlation with eGFR in most of the studies with respect to the assessment of renal dysfunction using BOLD [32, 33], except in the Michaely's study [34]. This contradiction was attributed to the fact that renal tissue oxygenation may depend not only on the severity of CKD but also on the etiology of the underlying kidney disease [30].

The role of SWI in evaluating renal dysfunction has been explored in two studies [6, 9]. Both perfusion alterations and tissue fibrosis resulted in SWI signal changes [9]. The feasibility of performing SWI on human kidney was investigated in 2010 for the first time [35]. Soon after, SWI was applied for assessing renal impairment in animal models by Pan and Zhang [6, 9]. In Pan's study, SWI score decreased and returned to baseline over 48 h after renal ischemia-reperfusion injury. In Zhang's study, the kidney/muscle signal ratio on SWI gradually decreased and was correlated with the pathologic fibrosis score over 8 weeks following unilateral ureteral obstruction [6]. However, to our knowledge, a comparison of BOLD and SWI for assessing renal impairment or dysfunction has not been performed previously. In this study, SWI showed a similar capacity to BOLD for assessing renal dysfunction.

In few studies, the renal dysfunction was assessed using both BOLD and DWI [36, 37]. However, the capacities of BOLD and DWI were not compared. In the current study, texture analysis showed significant changes in the non-sRI

Table 3 Comparison of selected texture features among the three groups

Group	sRI ($n = 31$)	non-sRI ($n = 24$)	CG ($n = 17$)	F	p
DWI					
0.25Quantile	1769 ± 142.6*#	1990 ± 185.1#	1990 ± 155.6*	16.71	< 0.001
0.5Quantile	1889 ± 154.5*#	2108 ± 197.5#	2087 ± 167.6*	13.13	< 0.001
Homogeneity	0.282 ± 0.135*#	0.541 ± 0.241#	0.518 ± 0.263*	12.75	< 0.001
BOLD					
Entropy	6.277 ± 0.506*	6.353 ± 0.446$	6.725 ± 0.278*$	5.913	0.004
SWI					
Skewness	− 0.356 ± 0.699*	− 0.109 ± 0.721	0.198 ± 0.402*	4.021	0.022
Correlation	0.534 ± 0.202*	0.561 ± 0.204$	0.700 ± 0.143*$	4.379	0.016

BOLD blood oxygen level–dependent MRI, *CG* control group, *DWI* diffusion-weighted imaging, *eGFR* estimated glomerular filtration rate, *non-sRI* non-severe renal function impairment, *sRI* severe renal function impairment

*, #, and $ show a significant difference in each row tested using a Student-Newman-Keuls

group compared with CG, rather detected by BOLD than by DWI. This was in line with Ichikawa's study, where the renal dysfunction was assessed using DWI with multi-b-factors. In this study, the cortical fast diffusion coefficient derived from the low b-factor-based DWI was reduced in the group of patients with mild renal dysfunction (eGFR = 60–80 mL/min/1.73 m^2) compared with the control group (eGFR > 80 mL/min/1.73 m^2) [21]. The conclusion was that the reduced renal perfusion played an important role in the initial progression of renal function impairment [21].

Assessment of tissue heterogeneity using texture analysis has recently emerged as a practical tool. In liver fibrosis quantification, several studies have suggested that increasing heterogeneity on CT or MRI was correlated with the stage of hepatic fibrosis [38, 39]. Owing to the heterogeneity of renal structure (being composed of the renal cortex, medulla, and papilla) on both anatomical and functional images, texture analysis may play an important role in characterizing renal dysfunction and (or) impairment. In the current study, several texture features of the kidney based on DWI, BOLD, and SWI were correlated with eGFR, opening the possibility to assess renal dysfunction with texture analysis of functional MRI.

This study has several limitations. Firstly, due to small sample size in the eGFR ranges of 30 to 60 mL/min/1.73 m^2, and 60 to 80 mL/min/1.73 m^2, the non-sRI group included patients with an eGFR in an expanded range of 30 to 80 mL/min/1.73 m^2. Secondly, a bi-exponential fitting model is not performed on free-breathing DWI with multiple b-factors. Thirdly, while the biomarker-based eGFR was based on bilateral renal function, the texture features were measured for the right kidney because there was an assumption that the renal function was similar in each split kidney. Finally, the cost and time effectiveness of MRI was relatively low in assessing renal dysfunction.

This study opens the door for further exploring texture analysis based on functional MRI as a tool for assessment of renal dysfunction. Its capacity for assessing renal dysfunction may depend on the initial cause and type of pathological changes over the course of renal impairment. The texture

Table 4 Capacity of the selected texture features for discriminating non-sRI from sRI or CG

Imaging method or feature	Discrimination of sRI from non-sRI			Discrimination of non-sRI from CG		
	AUC (95% CI)	*Z*	*p*	*AUC* (95% CI)	*Z*	*p*
DWI						
0.25Quantile	0.827 (0.701–0.915)	5.264	< 0.001	0.517 (0.356–0.676)	0.181	0.856
0.5Quantile	0.821 (0.694–0.911)	5.063	< 0.001	0.549 (0.386–0.705)	0.525	0.600
Homogeneity	0.840 (0.716–0.925)	6.298	< 0.001	0.561 (0.396–0.716)	0.623	0.533
BOLD						
Entropy	0.535 (0.395–0.671)	0.431	0.667	0.752 (0.593–0.874)	3.349	< 0.001
SWI						
Skewness	0.591 (0.451–0.722)	1.148	0.251	0.647 (0.482–0.790)	1.683	0.092
Correlation	0.531 (0.392–0.667)	0.384	0.701	0.701 (0.538–0.834)	2.396	0.017

AUC area under the receiver operating characteristic curve, *BOLD* blood oxygen level–dependent MRI, *CG* control group, *CI* confidence interval, *DWI* diffusion-weighted imaging, *eGFR* estimated glomerular filtration rate, *non-sRI* non-severe renal function impairment, *sRI* severe renal function impairment, *SWI* susceptibility-weighted imaging

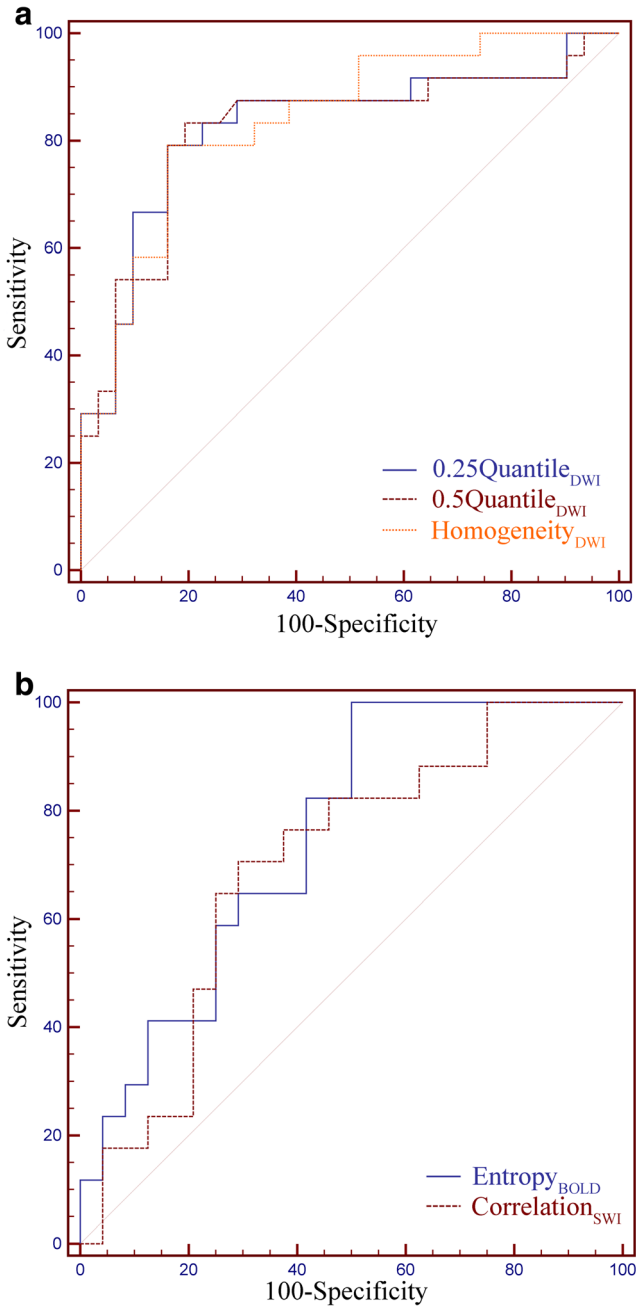

Fig. 3 Receiver operating characteristic curves of the selected texture features to differentiate non-severe renal function impairment (non-sRI) from severe renal function impairment (sRI) or control group (CG). **a** To discriminate non-sRI from sRI, the area under the receiver operating characteristic curve (AUC) was not significantly different between $0.25Quantile_{DWI}$ and $0.5Quantile_{DWI}$ ($Z = 0.528$, $p = 0.598$), between $0.25Quantile_{DWI}$ and $Homogeneity_{DWI}$ ($Z = 0.439$, $p = 0.661$), and between $0.5Quantile_{DWI}$ and $Homogeneity_{DWI}$ ($Z = 0.648$, $p = 0.517$). **b** To discriminate non-sRI from CG, no significant difference of AUC between $Entropy_{BOLD}$ and $Correlation_{SWI}$ was observed ($Z = 0.421$, $p = 0.674$)

features based on BOLD and SWI may be more suitable for assessing renal dysfunction during early stages because reduced renal perfusion plays an important role in the initial progression of renal impairment.

Funding This work was supported by the National Natural Science Foundation of China (81771798, 81771805); Jiangsu Provincial Medical Youth Talent Program, China (QNRC2016299); General Program of Jiangsu Provincial Commission of Health and Family Planning, China (H2017003); Key Project of Health Commission of Changzhou, Jiangsu, China (ZD201509); Applied and Basic Research Program of Science and Technology Bureau of Changzhou, Jiangsu, China (CJ20160038); and Changzhou Municipal Medical Youth Talent Program, Jiangsu, China (QN201610).

Compliance with ethical standards

Guarantor The scientific guarantor of this publication is Wei Xing.

Conflict of interest The authors of this manuscript declare no relationships with any companies, whose products or services may be related to the subject matter of the article.

Statistics and biometry Bin Xu kindly provided statistical advice for this manuscript.

Informed consent Written informed consent was obtained from all subjects (patients) in this study.

Ethical approval This study was approved by Ethics Committee of Third Affiliated Hospital of Soochow University.

Methodology
- retrospective
- cross-sectional study
- performed at one institution

References

1. Webster AC, Nagler EV, Morton RL, Masson P (2017) Chronic kidney disease. Lancet 389:1238–1252
2. Saran R, Li Y, Robinson B et al (2015) US renal data system 2014 annual data report: epidemiology of kidney disease in the United States. Am J Kidney Dis 66(Svii):S1–S305
3. Fine LG, Norman JT (2008) Chronic hypoxia as a mechanism of progression of chronic kidney diseases: from hypothesis to novel therapeutics. Kidney Int 74:867–872
4. Hirakawa Y, Tanaka T, Nangaku M (2017) Renal hypoxia in CKD; pathophysiology and detecting methods. Front Physiol 8:99
5. Takahashi T, Wang F, Quarles CC (2015) Current MRI techniques for the assessment of renal disease. Curr Opin Nephrol Hypertens 24:217–223
6. Zhang JG, Xing ZY, Zha TT et al (2017) Longitudinal assessment of rabbit renal fibrosis induced by unilateral ureteral obstruction using two-dimensional susceptibility weighted imaging. J Magn Reson Imaging 47:1572–1577
7. Abou-El-Ghar ME, El-Diasty TA, El-Assmy AM, Refaie HF, Refaie AF, Ghoneim MA (2012) Role of diffusion-weighted MRI in diagnosis of acute renal allograft dysfunction: a prospective preliminary study. Br J Radiol 85:e206–e211
8. Chang K, Barnes S, Haacke EM, Grossman RI, Ge Y (2014) Imaging the effects of oxygen saturation changes in voluntary apnea and hyperventilation on susceptibility-weighted imaging. AJNR Am J Neuroradiol 35:1091–1095
9. Pan L, Chen J, Xing W et al (2017) Magnetic resonance imaging evaluation of renal ischaemia-reperfusion injury in a rabbit model. Exp Physiol 102:1000–1006

10. Castellano G, Bonilha L, Li LM, Cendes F (2004) Texture analysis of medical images. Clin Radiol 59:1061–1069
11. Ortiz-Ramón R, Larroza A, Ruiz-España S, Arana E, Moratal D (2018) Classifying brain metastases by their primary site of origin using a radiomics approach based on texture analysis: a feasibility study. Eur Radiol. https://doi.org/10.1007/s00330-018-5463-6
12. Hocquelet A, Auriac T, Perier C et al (2018) Pre-treatment magnetic resonance-based texture features as potential imaging biomarkers for predicting event free survival in anal cancer treated by chemoradiotherapy. Eur Radiol. https://doi.org/10.1007/s00330-017-5284-z
13. Naganawa S, Enooku K, Tateishi R et al (2018) Imaging prediction of nonalcoholic steatohepatitis using computed tomography texture analysis. Eur Radiol. https://doi.org/10.1007/s00330-017-5270-5
14. American Diabetes Association (2013) Diagnosis and classification of diabetes mellitus. Diabetes Care 36(Suppl 1):S67–S74
15. Zhou HY, Chen TW, Zhang XM (2016) Functional magnetic resonance imaging in acute kidney injury: present status. Biomed Res Int 2016:2027370
16. Zhang L, Fried DV, Fave XJ, Hunter LA, Yang J, Court LE (2015) IBEX: an open infrastructure software platform to facilitate collaborative work in radiomics. Med Phys 42:1341–1353
17. Peng W, Liu C, Xia S et al (2017) Thyroid nodule recognition in computed tomography using first order statistics. Biomed Eng Online 16:67
18. Alobaidli S, McQuaid S, South C, Prakash V, Evans P, Nisbet A (2014) The role of texture analysis in imaging as an outcome predictor and potential tool in radiotherapy treatment planning. Br J Radiol 87:20140369
19. Woo S, Cho JY, Kim SY, Kim SH (2014) Histogram analysis of apparent diffusion coefficient map of diffusion-weighted MRI in endometrial cancer: a preliminary correlation study with histological grade. Acta Radiol 55:1270–1277
20. Xu X, Fang W, Ling H, Chai W, Chen K (2010) Diffusion-weighted MR imaging of kidneys in patients with chronic kidney disease: initial study. Eur Radiol 20:978–983
21. Ichikawa S, Motosugi U, Ichikawa T, Sano K, Morisaka H, Araki T (2013) Intravoxel incoherent motion imaging of the kidney: alterations in diffusion and perfusion in patients with renal dysfunction. Magn Reson Imaging 31:414–417
22. Hueper K, Rong S, Gutberlet M et al (2013) T2 relaxation time and apparent diffusion coefficient for noninvasive assessment of renal pathology after acute kidney injury in mice: comparison with histopathology. Invest Radiol 48:834–842
23. Mao W, Zhou J, Zeng M et al (2018) Intravoxel incoherent motion diffusion-weighted imaging for the assessment of renal fibrosis of chronic kidney disease: a preliminary study. Magn Reson Imaging 47:118–124
24. Müller MF, Prasad PV, Bimmler D, Kaiser A, Edelman RR (1994) Functional imaging of the kidney by means of measurement of the apparent diffusion coefficient. Radiology 193:711–715
25. Sigmund EE, Vivier PH, Sui D et al (2012) Intravoxel incoherent motion and diffusion-tensor imaging in renal tissue under hydration and furosemide flow challenges. Radiology 263:758–769
26. Li LP, Tan H, Thacker JM et al (2017) Evaluation of renal blood flow in chronic kidney disease using arterial spin labeling perfusion magnetic resonance imaging. Kidney Int Rep 2:36–43
27. Gillis KA, McComb C, Patel RK et al (2016) Non-contrast renal magnetic resonance imaging to assess perfusion and corticomedullary differentiation in health and chronic kidney disease. Nephron 133:183–192
28. Chen WB, Liang L, Zhang B et al (2015) To evaluate the damage of renal function in CIAKI rats at 3T: using ASL and BOLD MRI. Biomed Res Int 2015:593060
29. Odudu A, Francis ST, McIntyre CW (2012) MRI for the assessment of organ perfusion in patients with chronic kidney disease. Curr Opin Nephrol Hypertens 21:647–654
30. Neugarten J (2012) Renal BOLD-MRI and assessment for renal hypoxia. Kidney Int 81:613–614
31. Rapacchi S, Smith RX, Wang Y et al (2015) Towards the identification of multi-parametric quantitative MRI biomarkers in lupus nephritis. Magn Reson Imaging 33:1066–1074
32. Inoue T, Kozawa E, Okada H et al (2011) Noninvasive evaluation of kidney hypoxia and fibrosis using magnetic resonance imaging. J Am Soc Nephrol 22:1429–1434
33. Milani B, Ansaloni A, Sousa-Guimaraes S et al (2017) Reduction of cortical oxygenation in chronic kidney disease: evidence obtained with a new analysis method of blood oxygenation level-dependent magnetic resonance imaging. Nephrol Dial Transplant 32:2097–2105
34. Michaely HJ, Metzger L, Haneder S, Hansmann J, Schoenberg SO, Attenberger UI (2012) Renal BOLD-MRI does not reflect renal function in chronic kidney disease. Kidney Int 81:684–689
35. Mie MB, Nissen JC, Zöllner FG et al (2010) Susceptibility weighted imaging (SWI) of the kidney at 3T–initial results. Z Med Phys 20:143–150
36. Park SY, Kim CK, Park BK, Kim SJ, Lee S, Huh W (2014) Assessment of early renal allograft dysfunction with blood oxygenation level-dependent MRI and diffusion-weighted imaging. Eur J Radiol 83:2114–2121
37. Li X, Xu X, Zhang Q et al (2014) Diffusion weighted imaging and blood oxygen level-dependent MR imaging of kidneys in patients with lupus nephritis. J Transl Med 12:295
38. Daginawala N, Li B, Buch K et al (2016) Using texture analyses of contrast enhanced CT to assess hepatic fibrosis. Eur J Radiol 85:511–517
39. Yu H, Buch K, Li B et al (2015) Utility of texture analysis for quantifying hepatic fibrosis on proton density MRI. J Magn Reson Imaging 42:1259–1265